LETTER TO THE EDITOR

Structural insights into ligand binding and activation of the human thyrotropin-releasing hormone receptor

Cell Research (2022) 32:855–857; https://doi.org/10.1038/s41422-022-00641-x

Dear Editor,

The thyrotropin-releasing hormone (TRH) is the initial hormone of the hypothalamo–pituitary–thyroid axis (HPT), a signaling cascade required for metabolic homeostasis and development in vertebrates. TRH is a tripeptide hormone (pGlu–His–Pro-NH2) that is synthesized in the hypothalamus and activates thyrotropin-releasing hormone receptor (TRHR), a member of class A G protein-coupled receptor (GPCR). Activated TRHR couples to G_q and activates the phosphatidylinositol (IP3)-calcium-protein kinase C (PKC) pathway[1] that ultimately leads to upregulation of thyroid hormones.

TRHR is mainly expressed in thyroid-stimulating hormone (TSH, thyrotropin)-secreting cells located at the pituitary. In chicken and mouse, there are three and two subtypes of TRHR, respectively.[2,3] By contrast, only one single type of TRHR exists in humans, which is closer to TRHR1 than TRHR2 in mouse.[4] TRH plays a multifunctional role in the central nervous system, particularly in the regulation of thyroid hormone homeostasis along the HPT axis. Upon stimulation by TRH, TRHR prompts TSH production, which then induces the synthesis of thyroid hormones (Fig. 1a). Moreover, Taltirelin, a synthetic TRH analog has been approved for the treatment of spinocerebellar degeneration (SCD) in Japan.[5] However, research on other TRH derivatives, including montirelin, thymoliberin, posatirelin, and azetirelin dihydrate were terminated. One of the important reasons is the lack of structural information, especially on how TRH recognizes and activates TRHR. Here we report the cryo-EM structure of the human TRHR bound to TRH and G protein at 3.0 Å resolution, which reveals detailed mechanism underlying TRH recognition and TRHR activation, and provides a rational model for drug design targeting TRHR.

The structure of the TRH-bound TRHR was determined with a modified version of G_q as reported previously[6–8] and described in methods. In addition, we used NanoBiT tethering strategy, which has been used to determine the structures of many GPCR–G protein complexes,[8–10] to facilitate the assembly of the TRH–TRHR–G_q complex (Supplementary information, Fig. S1a). The cryo-EM density map is of high quality, enabling us to build the final structure model, which is comprised of TRH, TRHR (residues Q25$^{1.32}$ to N336$^{8.59}$ based on Ballesteros–Weinstein numbering), three subunits of the modified G_q and scFv16.

The overall assembly of the TRH–TRHR–G_q complex adopts a typical arrangement of class A GPCR–G protein complexes, with TRHR forming a canonical seven transmembrane helical domain (TMD) (Fig. 1b, c; Supplementary information, Figs. S1, S2, and Table S1). Within this complex, TRH is docked into a Y-shaped TMD pocket formed by TM2, TM3, TM5–7, and ECL1–3 (Fig. 1d), in which the tripeptide side chains of TRH (amide L-pyroglutamyl–L-histidyl–L-prolineamide) make extensive interactions with the receptor as summarized in Supplementary information, Fig. S3a and b. The TRHR pocket is amphipathic, with one side enriched with positively charged residues of R185$^{5.32}$ and R306$^{7.39}$, and the other side enriched with hydrophobic residues of W160$^{4.60}$, L164$^{4.64}$, and Y181^{ECL2} (Fig. 1e, f; Supplementary information, Fig. S3a, b). All four carbonyl groups of TRH are faced against the positively charged surface of the pocket, whereas the pyrrole ring of TRH is docked into a hydrophobic cavity formed by residues I109$^{3.36}$, Y282$^{6.51}$, and I309$^{7.42}$ (Fig. 1g; Supplementary information and Fig. S3a, b). In addition, the imidazole ring of histidine from TRH fits into the cavity formed by Y106$^{3.33}$, W160$^{4.60}$, Y181^{ECL2}, and Y192$^{5.39}$ (Fig. 1f). Consistent with this observed binding mode of TRH, mutations at the key pocket residues, including Y106$^{3.33}$, W160$^{4.60}$, Y181^{ECL2}, all result in dramatic decrease of TRH-induced receptor activation (Fig. 1l). In addition, based on the TRH-bound TRHR structure, synthetic TRHR ligands, including Taltirelin and the clinical candidate, montirelin, can be easily modeled into the TRHR ligand-binding pocket (Supplementary information, Fig. S3c).

A comparison of our TRH-bound TRHR structure with the antagonist-bound CCKAR structure[11] (PDB code: 7F8U) reveals the underlying mechanism of TRH-induced TRHR activation. Compared with the inactive CCKAR, the TM6 cytoplasmic end of TRHR undertakes a pronounced outward displacement, as well as a lateral shift of TM5 and a slightly inward movement of TM7 (Fig. 1h, i), which are the conserved conformational changes upon class A GPCR activation.[12] TRH makes direct contacts with Y282$^{6.51}$, which initiates ligand-binding signal propagation to the intracellular surface of TRHR by inducing the conformational change of the highly conserved "toggle-switch" residue W279$^{6.48}$, which is located at one helical turn below Y282$^{6.51}$. In addition, the C-terminus of TRH (specific pyrrole ring) forms a hydrophobic network with I109$^{3.36}$ and I309$^{7.42}$ (Fig. 1j), two residues located at the bottom of the TRH-binding pocket and directly contact with W279$^{6.48}$. The alanine mutation at residues Y282$^{6.51}$, I109$^{3.36}$, and I309$^{7.42}$ dramatically reduced TRHR activity, supporting that these residues are important for TRHR activation (Fig. 1l; Supplementary information, Fig. S4 and Table S2). We also observed conformational changes in other conserved "micro-switch" motifs, including PIF, DRY, and NPxxY (Supplementary information, Fig. S5). Notably, the isoleucine of the classical "PIF" motif is substituted by S113$^{3.40}$ but it retained a similar function, which also occurs in the V2R structure.[13] In addition, the swing of indole ring of W279$^{6.48}$ further facilitates the swing of F$^{6.44}$ and the outward shift of TM6. The notable outward displacement of the cytoplasmic end of TM6 opens a cytoplasmic cavity, together with TM2, TM3, TM5, TM7, and helix 8, to accommodate the C-terminal α5 helix of $G\alpha_q$.

Abnormal mutations of TRHR have been shown to associate with central congenital hypothyroidism (CCH) and short stature in childhood, which is underdiagnosed. The structure of the TRH–TRHR–G_q complex provides a basis for understanding pathogenesis caused by disease-associated mutations. We mapped all the reported mutations onto our structure and found that these disease-associated mutations are located in three major

Received: 19 December 2021 Accepted: 23 February 2022
Published online: 1 April 2022

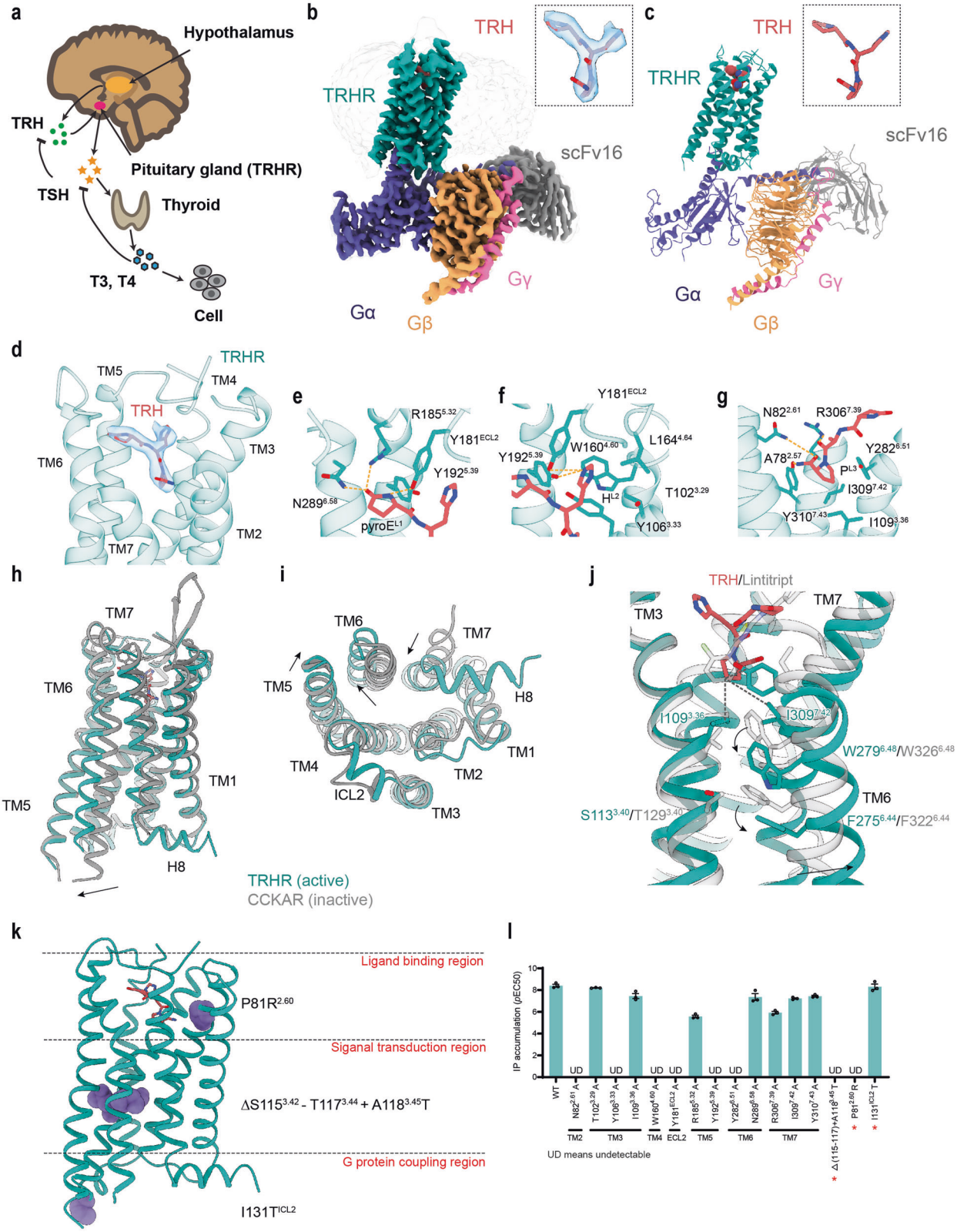

regions of TRHR: the ligand-binding pocket, the G protein-coupling site, and the central region connecting these two regions (Fig. 1k). The first patient case with prolonged neonatal jaundice was found with a homozygous missense mutation at position P81$^{2.60}$ to an arginine (p.P8$^{2.60}$R), which is closed to the ligand-binding pocket.[14] Modeling of the P81R$^{2.60}$ mutation indicates that the side chain of arginine might interact with N82$^{2.61}$ to interfere with the binding of TRH. The second patient case contains a compound heterozygote, with one allele stopped at R17 (p.R17X), and the other allele with an inframe deletion from position S115$^{3.42}$ to position T117$^{3.44}$ plus an A118$^{3.45}$T mutation (p.ΔS115$^{3.42}$–T117$^{3.44}$ + p.A118$^{3.45}$T).[15] These mutations resulted in

Fig. 1 Cryo-EM structure of the TRH–TRHR–G_q complex. a Schematic diagram of the hypothalamo–pituitary–thyroid axis. Briefly, hypothalamus secrete TRH, which could stimulate the pituitary to release TSH. TSH further acts at the thyroid to stimulate the synthesis and secretion of pro-hormone thyroxin (T4) and triiodothyronine (T3). The secretion of TRH and TSH can be controlled by T4 and T3 in a negative feedback loop to maintain physiological levels of the main hormones of the HPT axis. **b** Orthogonal view of the density map. TRHR, green; TRH, red; $G\alpha_q$, purple; Gβ, orange; Gγ, violet; scFv16, gray. The density of TRH is highlighted. **c** Structural model of the TRH–TRHR–G_q complex. All subunits and TRH are colored as in **b**. **d** TRH-binding pocket in TRHR. TRHR is shown as cartoons, and the cryo-EM density of TRH is shown with the stick model of TRH fitted in. **e**–**g** Detailed interactions of three TRH groups, L-prolineamide (**e**), L-histidyl (**f**), and L-pyroglutamyl (**g**) with residues in TRHR, respectively. **h**–**j** Structural superposition of TRHR and the inactive CCKAR. Side view (**h**); cytoplasmic view (**i**); TRH-trigged conformation changes of $W279^{6.48}$ and $F275^{6.44}$ (**j**). TRHR, green; CCKAR, gray. **k** The disease-associated TRHR mutations. Mutations are shown as magenta spheres. **l** Alanine mutagenesis analysis of the TRH-binding pocket of TRHR and analysis of disease-associated TRHR mutations. The IP-1 assay was performed to evaluate the effects of TRH on the G_q-coupling activity of TRHR. Data were analyzed using a three-parameter logistic equation to determine pEC_{50}. Data are shown as means ± SEM from six (wild-type) or three (variants) independent experiments. Disease-associated TRHR mutations are indicated with red stars. UD, undetectable.

a receptor with a truncated TM3, possibly a non-functional receptor. The third case harbors a threonine replacement of $I131^{ICL2}$, which makes hydrophobic interactions with residues in the αN–α5 cleft of the $G\alpha_q$ subunit. Consistently, introducing these disease-associated mutations into TRHR resulted in loss of potency (first and second case mutations) or efficacy (third case mutation) (Fig. 1l; Supplementary information, Fig. S4 and Table S3) of TRH-induced TRHR activation.

In summary, we have solved the cryo-EM structure of the human TRHR in complex with TRH and G_q, which provides details of how the endogenous ligand TRH inserts into the relative hydrophilic binding pocket. Each amino acid group from the TRH tripeptide binds to the different cavities in the receptor, which ultimately results in TRHR conformational changes and coupling of downstream G_q signaling. Site-directed mutagenesis studies have further confirmed the mode of TRH binding and the mechanism of TRHR activation by TRH. Our structure also provides a template to model other THRH ligands and allows us to understand the basis of the disease-associated mutations of TRHR.

Youwei Xu[1,5]✉, Hongmin Cai[1,5], Chongzhao You[1,2], Xinheng He[1,2], Qingning Yuan[1], Hualiang Jiang[1,2,3,4], Xi Cheng[1,4], Yi Jiang[1] and H. Eric Xu[1,2,3]✉

[1]*The CAS Key Laboratory of Receptor Research, Shanghai Institute of Materia Medica, Chinese Academy of Sciences, Shanghai, China.* [2]*University of Chinese Academy of Sciences, Beijing, China.* [3]*School of Life Science and Technology, ShanghaiTech University, Shanghai, China.* [4]*State Key Laboratory of Drug Research and CAS Key Laboratory of Receptor Research, Shanghai Institute of Materia Medica, Chinese Academy of Sciences, Shanghai, China.* [5]*These authors contributed equally: Youwei Xu, Hongmin Cai.*
✉*email: xuyouwei@simm.ac.cn; eric.xu@simm.ac.cn*

DATA AVAILABILITY

The corresponding coordinates and cryo-EM density map have been deposited in the Protein Data Bank (http://www.rcsb.org/pdb) with code 7WKD, and in EMDB (http://www.ebi.ac.uk/pdbe/emdb/) with code EMD-32565.

REFERENCES

1. Hinkle, P. M., Gehret, A. U. & Jones, B. W. *Front. Neurosci.* **6**, 180 (2012).
2. Li, X. et al. *Poult. Sci.* **99**, 1643–1654 (2020).
3. Sun, Y., Lu, X. & Gershengorn, M. C. *J. Mol. Endocrinol.* **30**, 87–97 (2003).
4. Matre, V. et al. *Biochem. Biophys. Res. Commun.* **195**, 179–185 (1993).
5. Brown, W. M. *IDrugs* **4**, 1389–1400 (2001).
6. Nehme, R. et al. *PLoS One* **12**, e0175642 (2017).
7. Koehl, A. et al. *Nature* **558**, 547–552 (2018).
8. Yin, Y. L. et al. *Nat. Struct. Mol. Biol.* **28**, 755–761 (2021).
9. Duan, J. et al. *Nat. Commun.* **11**, 4121 (2020).
10. Zhou, F. et al. *Nat. Commun.* **11**, 5205 (2020).
11. Zhang, X. et al. *Nat. Chem. Biol.* **17**, 1230–1237 (2021).
12. Liu, Q. et al. *Nat. Chem. Biol.* **17**, 1238–1244 (2021).
13. Zhou, F. et al. *Cell Res.* **31**, 929–931 (2021).
14. Koulouri, O. et al. *J. Clin. Endocrinol. Metab.* **101**, 847–851 (2016).
15. Collu, R. et al. *J. Clin. Endocrinol. Metab.* **82**, 1561–1565 (1997).

ACKNOWLEDGEMENTS

We thank Kai Wu and Wen Hu from Advanced Center for Electron Microscopy at Shanghai Institute of Materia Medica, Chinese Academy of Sciences for providing technical support and assistance during data collection, Yuqi Ping from our laboratory for the suggestions and critical reading during manuscript preparation. This work was partially supported by the Ministry of Science and Technology of China (2018YFA0507002), the National Natural Science Foundation of China (32130022), Shanghai Municipal Science and Technology Major Project (2019SHZDZX02), Shanghai Municipal Science and Technology Major Project, CAS Strategic Priority Research Program (XDB37030103) to H.E.X.; Fund of Youth Innovation Promotion Association (2018319 Y8G7011009) to X.C.; Science and Technology Commission of Shanghai Municipal (20431900100) and Jack Ma Foundation (2020-CMKYGG-05) to H. J.; the National Natural Science Foundation (31770796) and National Science and Technology Major Project (2018ZX09711002) to Y.J.; the National Natural Science Foundation of China (81902085), and Key tasks of LG laboratory (LG202101-01-03) to Y.X.

AUTHOR CONTRIBUTIONS

Y.X. prepared samples for cryo-EM grid preparation; Q.Y. performed cryo-EM data collection; Y.X. processed the cryo-EM data, built the model, and refined the structure model. H.C. conducted functional studies and data analysis; C.Y. prepared the figures, performed the structural analysis; X.H. carried out docking analysis; X.C. and H.J. were responsible for molecular docking studies and writing of methods; Y.J. participated in the supervision of this research, fund acquisition, structural analysis, and manuscript editing; H.E.X. and Y.X. conceived and supervised the project; H.E.X. and Y.X. prepared the manuscript with the input from all authors.

COMPETING INTERESTS

The authors declare no competing interests.

ADDITIONAL INFORMATION

Supplementary information The online version contains supplementary material available at https://doi.org/10.1038/s41422-022-00641-x.

Correspondence and requests for materials should be addressed to Youwei Xu or H. Eric Xu.

Reprints and permission information is available at http://www.nature.com/reprints